Supporting Information

Controlled Construction of Cu(I) Sites within Confined Spaces via Host-Guest Redox: Highly Efficient Adsorbents for Selective CO Adsorption

Yu-Xia Li,[†] *Yu-Nong Ji,*[†] *Meng-Meng Jin,*[†] *Shi-Chao Qi,*[†] *Shuai-Shuai Li,*[†] *Ding-Ming Xue,*[†] *Ming Bo Yue,*[‡] *Xiao-Qin Liu,**[,†] *and Lin-Bing Sun**[,†]

†State Key Laboratory of Materials-Oriented Chemical Engineering, Jiangsu National Synergetic Innovation Center for Advanced Materials (SICAM), College of Chemical Engineering, Nanjing Tech University, Nanjing 210009, China. ‡School of Chemistry and Chemical Engineering, Qufu Normal University, Shandong, China

*Corresponding author. E-mail: liuxq@njtech.edu.cn; lbsun@njtech.edu.cn.

Contents

Materials Characterization.

Powder X-ray diffraction (XRD) patterns of the samples were collected using a BRUKER D8 Advance diffractometer equipped with Cu Kα radiation in the 2θ ranges from 2° to 60° at 40 kV and 30 mA. Morphologies of the materials were observed by field-emission scanning electron microscopy (FESEM; HITACHI S-4800). Transmission electron microscopy (TEM) was carried out on a JEM-200CX electron microscope at 200 kV. The N_2 adsorption isotherms were investigated from an ASAP 2020 system at –196 °C. Before the analysis, the samples (100 mg) were degassed at 180 °C for 4 h under vacuum. The Brunauer–Emmett–Teller (BET) surface area was identified by relative pressure ranging from 0.04 to 0.20. The total pore volume was analyzed by the uptake at a relative pressure of about 0.99. Fourier transform infrared (FTIR) measurements were conducted on a Nicolet Nexus 470 spectrometer using the KBr pellet technique. The spectra were recorded with a 2 cm^{-1} resolution. Adsorption of CO on adsorbents were investigated by low-pressure adsorption experiments monitored by Diffuse Reflectance Infrared Fourier Transform Spectroscopy (DRIFTS). The study was performed with a Nicolet NEXUS™ FT-IR spectrometer equipped with a liquid-nitrogen cooled MCT-A detector and an Ever-Glow mid-IR source and using a PIKE DiffuseIR™ diffuse reflectance accessory with a PIKE DiffuseIR™ high-temperature environmental chamber equipped with KBr windows. A home-built pressure control system employing a turbomolecular pump and an electronically actuated leaking-valve was connected to the chamber. It allowed evacuation of the measurement chamber to a base-pressure of 2×10^{-6} mbar and adjustment of constant probe molecule pressure up to 100 mbar. Thermogravimetric (TG) analysis was performed on a thermobalance (STA-499C, NETZSCH) in N_2 atmosphere with a flow rate of 10 $mL\cdot min^{-1}$ and sample (5 mg) was heated from 30 to 800 °C with a heating rate of 10 $°C\cdot min^{-1}$. X-ray photoelectron spectroscopy (XPS) analysis was determined by a Physical Electronic PHI 550 spectrometer with an Al Kα X-ray source (1486.6 eV).A wet chemistry titration method was applied to analyze the quantity of Fe^{2+} content in the samples. In a typical process, sample (200 mg) was added into the H_2O (50 mL) under continuous agitation. The consumption of ceric sulfate solution (0.1138 $mol\cdot L^{-1}$) can quantify the amount of Fe^{2+} by immediate titration, where phenanthroline was used as an indicator. A wet chemistry titration method was also applied to quantify of Cu^{+} content in the samples. Prior to the titration test, the ferric chloride reagent

need to be prepared. $FeCl_3$ (150 g) was dissolved in HCl (300 mL), H_2O (800 mL), and H_2O_2 (10 mL) and then the solution was heated till boiling for removing excess H_2O_2. After dropping to room temperature, a ferric chloride reagent can be obtained. Sample (200 mg) was added into the reagent (10 mL) under continuous agitation. Cu^{2+} and Fe^{2+} were produced by the reaction between Cu^{+} with Fe^{3+}. Then, H_2O (50 mL) was added to the mixture. The consumption of ceric sulfate solution (0.1138 $mol \cdot L^{-1}$) can quantify the total amount of Fe^{2+} by immediate titration, where phenanthroline was used as an indicator. The consumption of ceric sulfate solution minus the quantity of Fe^{2+} content is the quantity of Cu^{+} content.

Table S1 Structural properties and Cu contents of different samples

Sample	S_{BET} ($m^2 \cdot g^{-1}$)	V_p ($cm^3 \cdot g^{-1}$)	Cu^+ yield (%)
MIL-100(Fe)	2023	0.94	–
Cu(I)MFe-1	1531	0.82	99.1
Cu(I)MFe-2	1185	0.75	99.4
Cu(I)MFe-3	1067	0.65	99.6
Cu(I)MFe-4	924	0.63	99.5
Cu(I)MFe-3-I	988	0.46	99.3

Table S2 Adsorption amount of CO for some typical adsorbents

Adsorbent	*T* (K)	*P* (bar)	Adsorbed amount ($mmol \cdot g^{-1}$)	CO/N_2 Selectivity (IAST[a] / Equilibrium)	Ref.
Cu(I)MFe-3	298	1	3.75	424/31	This work
AC	303	1	0.39	–/1.2	[1]
Zeolite 13X	293	1	0.99	–/2.8	[2]
Zeolite 5A	303	1	1.0	–/2.0	[1,3]
ZSM-5	303	1	0.17	–/1.1	[4]
MIL-101(Cr)	288	1	1.13	–/3.7	[5]
MIL-125_NH_2	303	1	0.15	–/0.94	[6]
UTSA-16	298	1	0.11	–/0.44	[7]
Cu-BTC	295	1	0.8	–/2.0	[8]
MIL-100(Fe)	298	1	0.38	0.1/1.5	[9]
CuCl/AC	298	1	2.5	45/14	[10]
CuCl/γ-Al_2O_3	303	2	1.0	–/–	[3]
CuCl/NaY	303	0.7	2.3	–/2.8	[11]
CuCl/Y	303	1	2.67	–/26	[12]
CuZSM-5	303	1	0.11	–/–	[13]
CuCl/Polystyrene Resin	293	1	0.94	–/6.0	[14]
Cu_2O-modified SBA-15	298	1	0.48	–/6.7	[15]
CuCl/SBA-15	308	1	0.50	–/–	[16]
CuCl/MCM-41	308	1	0.57	–/–	[16]
Cu(I)@MIL-100(Fe)	298	1	2.78	280/4.3	[9]

[a] IAST selectivity at the $CO:N_2$ ratio of 0.33.

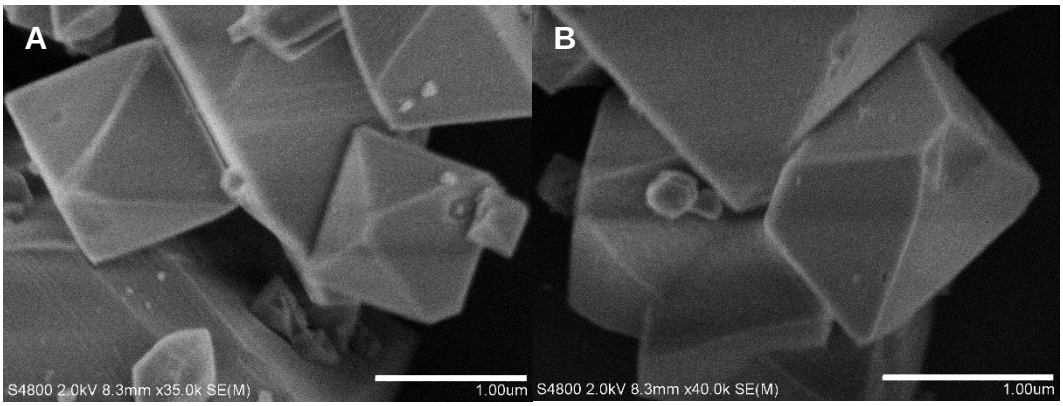

Figure S1. SEM images of (A) MIL-100(Fe) and (B) Cu(I)MFe-3. Scale bars represent 1 μm.

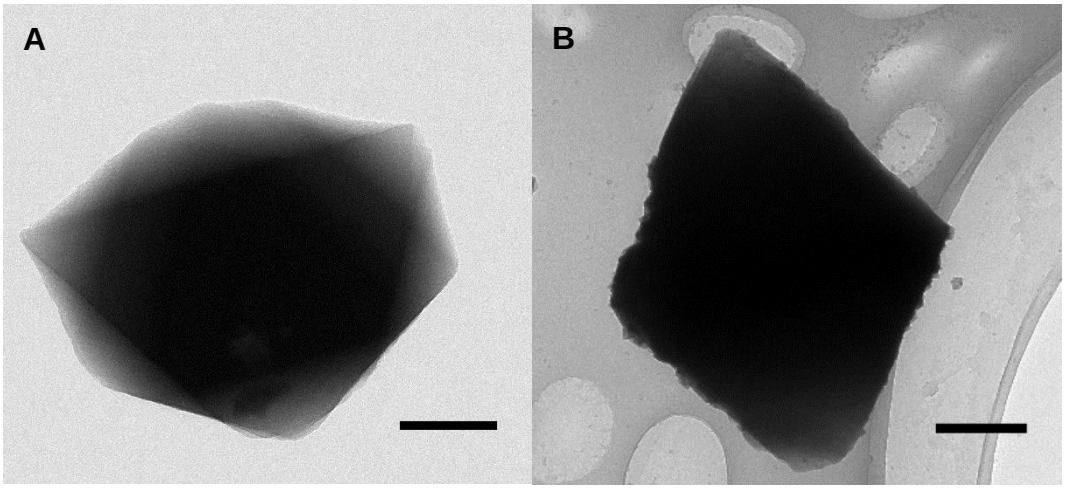

Figure S2. TEM images of (A) MIL-100(Fe) and (B) Cu(I)MFe-3. Scale bars represent 200 nm.

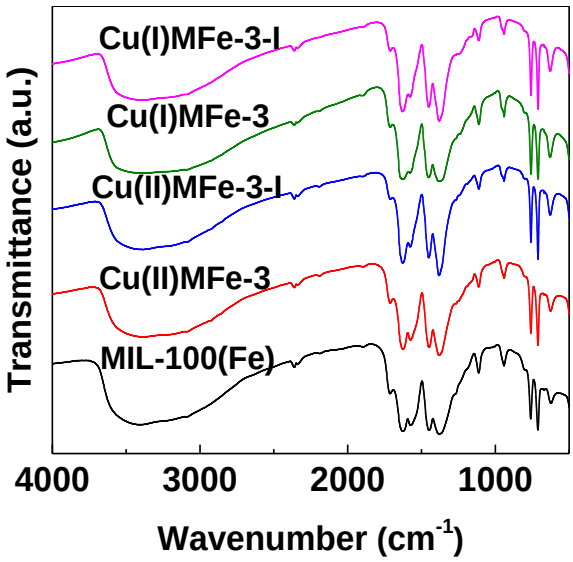

Figure S3. FT-IR spectra of the samples MIL-100(Fe) and Cu^{+}-containing MIL-100(Fe).

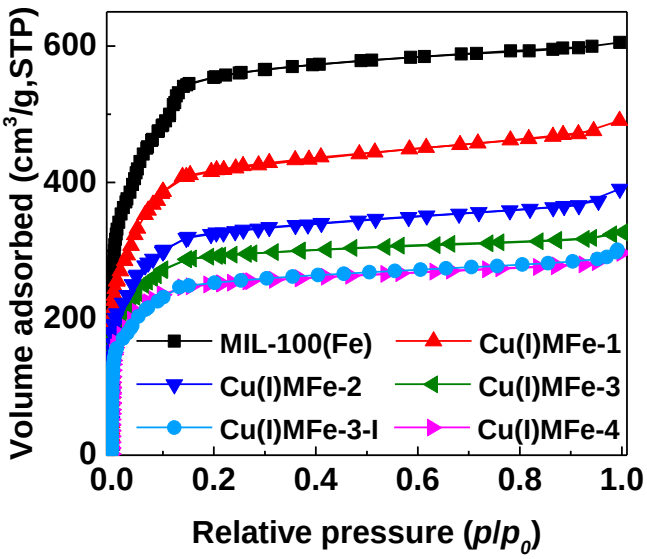

Figure S4. N_2 adsorption isotherms of MIL-100(Fe) and Cu^+-containing MIL-100(Fe).

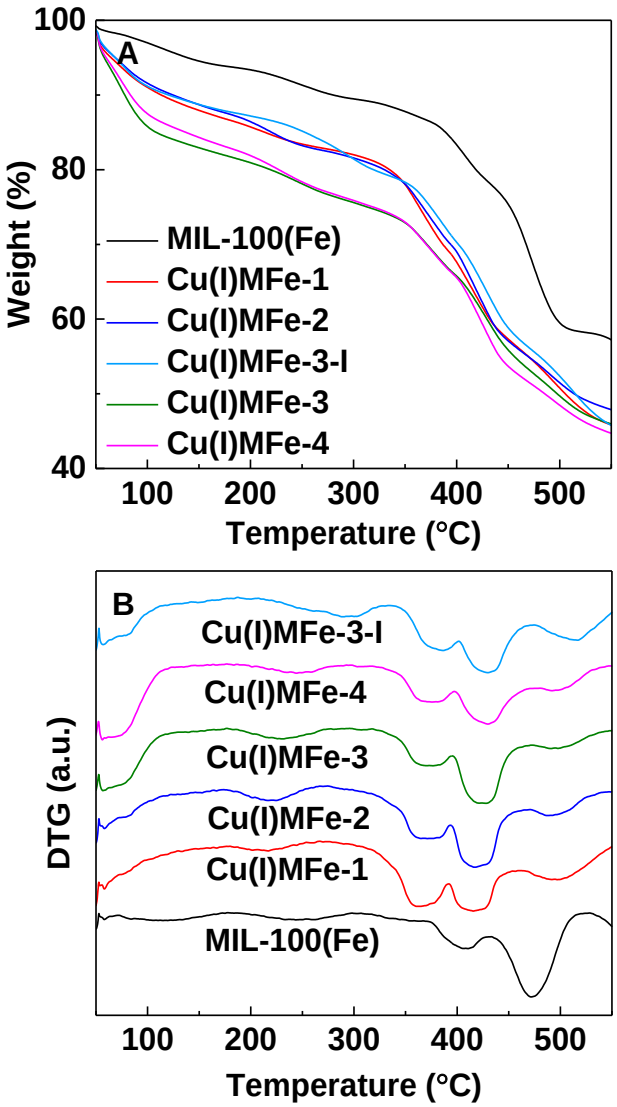

Figure S5. (A) TG and (B) DTG profiles of MIL-100(Fe) and Cu^{+}-containing MIL-100(Fe). DTG curves are plotted offset for clarity.

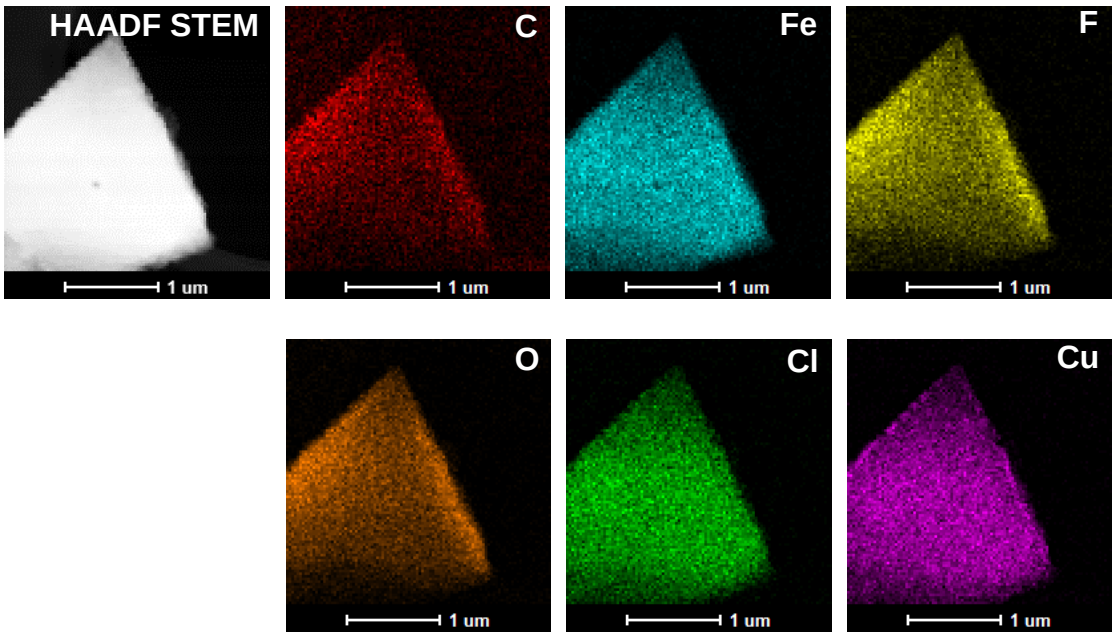

Figure S6. HAADF STEM and EDX mapping images of C, Fe, F, O, Cl, and Cu elements of the sample Cu(I)MFe-3.

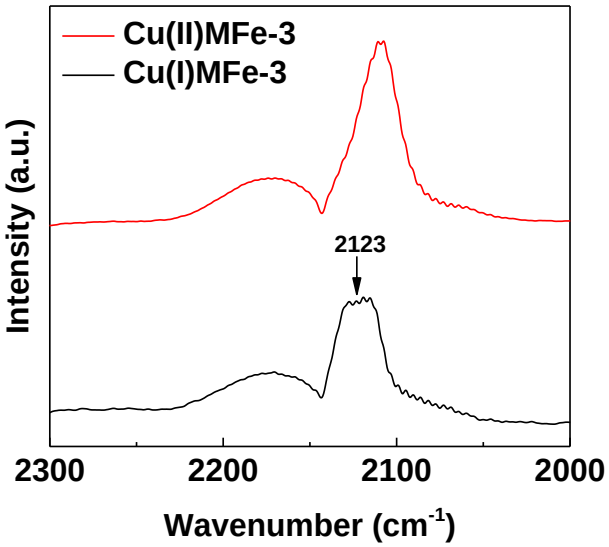

Figure S7. DRIFT spectra of CO adsorbed at 298 K on Cu(II)MFe-3 and Cu(I)MFe-3.

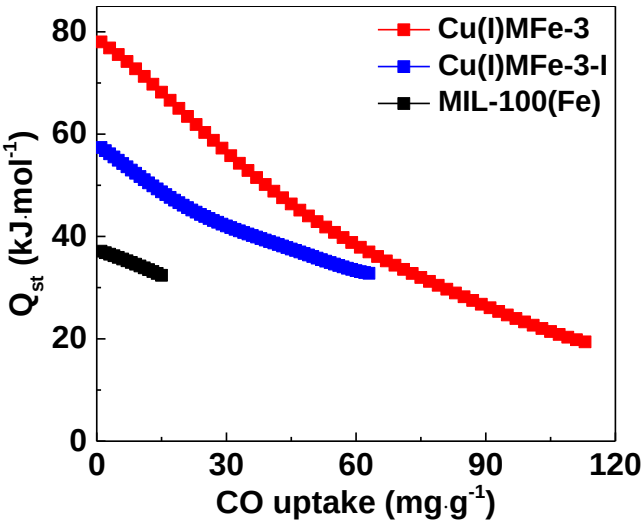

Figure S8. CO isosteric heat of adsorption of different samples.

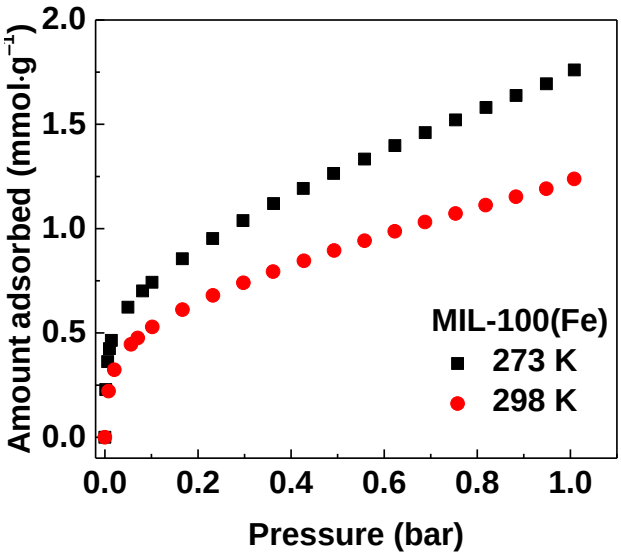

Figure S9. Adsorption isotherms of CO on MIL-100(Fe) at 273 and 298 K.

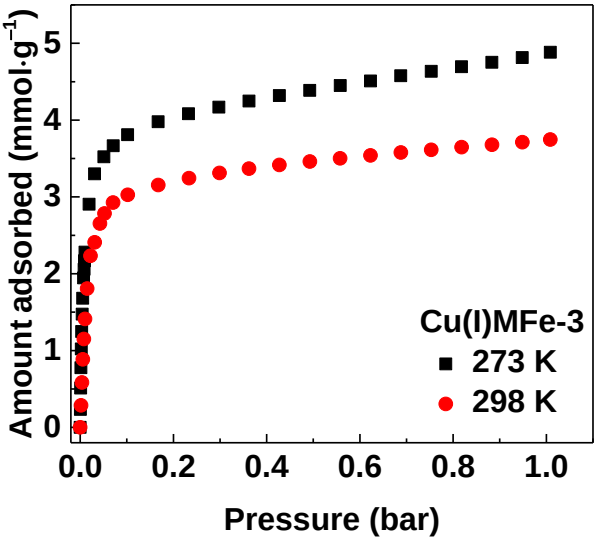

Figure S10. Adsorption isotherms of CO on Cu(I)MFe-3 at 273 and 298 K.

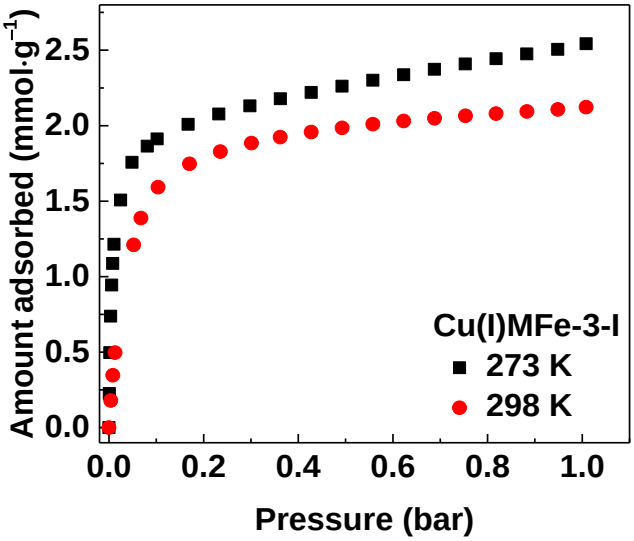

Figure S11. Adsorption isotherms of CO on Cu(I)MFe-3-I at 273 and 298 K.

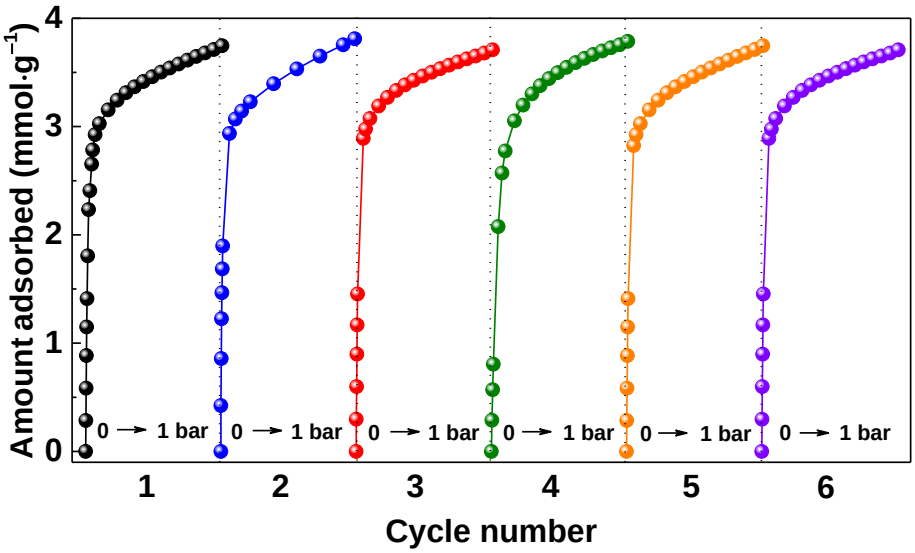

Figure S12. Cycling adsorption of CO over the adsorbent Cu(I)MFe-3 at 298 K and 1 bar.

References

(1) Sievers, W.; Mersmann, A. Single and Multicomponent Adsorption Equilibria of Carbon Dioxide, Nitrogen, Carbon Monoxide and Methane in Hydrogen Purification Processes *Chem. Eng. Technol.* **1994**, *17*, 325.

(2) Park, Y.; Ju, Y.; Park, D.; Lee, C. H. Adsorption Equilibria and Kinetics of Six Pure Gases on Pelletized Zeolite 13X up to 1.0 MPa: CO_2, CO, N_2, CH_4, Ar and H_2. *Chem. Eng. J.* **2016**, *292*, 348.

(3) Saha, D.; Deng, S. G. Adsorption Equilibria and Kinetics of Carbon Monoxide on Zeolite 5A, 13X, MOF-5, and MOF-177. *J. Chem. Eng. Data* **2009**, *54*, 2245.

(4) Heymans, N.; Alban, B.; Moreau, S.; De Weireld, G. Experimental and Theoretical Study of the Adsorption of Pure Molecules and Binary Systems Containing Methane, Carbon Monoxide, Carbon Dioxide and Nitrogen. Application to the Syngas Generation. *Chem. Eng. Sci.* **2011**, *66*, 3850.

(5) Munusamy, K.; Sethia, G.; Patil, D. V.; Rallapalli, P. B. S.; Somani, R. S.; Bajaj, H. C. Sorption of Carbon Dioxide, Methane, Nitrogen and Carbon Monoxide on MIL-101(Cr): Volumetric Measurements and Dynamic Adsorption Studies. *Chem. Eng. J.* **2012**, *195*, 359.

(6) Regufe, M. J.; Tarnajon, J.; Ribeiro, A. M.; Ferreira, A.; Lee, U. H.; Hwang, Y. K.; Chang, J. S.; Serre, C.; Loureiro, J. M.; Rodrigues, A. E. Syngas Purification by Porous Amino-Functionalized Titanium Terephthalate MIL-125. *Energy Fuels* **2015**, *29*, 4654.

(7) Agueda, V. I.; Delgado, J. A.; Uguina, M. A.; Brea, P.; Spjelkavik, A. I.; Blom, R.; Grande, C. Adsorption and Diffusion of H_2, N_2, CO, CH_4 and CO_2 in UTSA-16 Metal-Organic Framework Extrudates. *Chem. Eng. Sci.* **2015**, *124*, 159.

(8) Wang, Q. M.; Shen, D. M.; Bulow, M.; Lau, M. L.; Deng, S. G.; Fitch, F. R.; Lemcoff, N. O.; Semanscin, J. Metallo-Organic Molecular Sieve for Gas Separation and Purification. *Microporous Mesoporous Mater.* **2002**, *55*, 217.

(9) Peng, J.; Xian, S.; Xiao, J.; Huang, Y.; Xia, Q.; Wang, H.; Li, Z. A Supported Cu(I)@MIL-100(Fe) Adsorbent with High CO Adsorption Capacity and CO/N_2

Selectivity. *Chem. Eng. J.* **2015**, *270*, 282.

(10) Ma, J. H.; Li, L.; Ren, J.; Li, R. F. CO Adsorption on Activated Carbon-Supported Cu-Based Adsorbent Prepared by a Facile Route. *Sep. Purif. Technol.* **2010**, *76*, 89.

(11) Xie, Y. C.; Zhang, J. P.; Qiu, J. G.; Tong, X. Z.; Fu, J. P.; Yang, G.; Yan, H. J.; Tang, Y. Q. Zeolites Modified by CuCl for Separating CO from Gas Mixtures Containing CO_2. *Adsorption* **1996**, *3*, 27.

(12) Gao, F.; Wang, Y.; Wang, S. Selective Adsorption of CO on CuCl/Y Adsorbent Prepared Using $CuCl_2$ as Precursor: Equilibrium and Thermodynamics. *Chem. Eng. J.* **2016**, *290*, 418.

(13) Rakic, V.; Rac, V.; Dondur, V.; Auroux, A. Competitive Adsorption of N_2O and CO on CuZSM-5, FeZSM-5, CoZSM-5 and Bimetallic Forms of ZSM-5 Zeolite. *Catal. Today* **2005**, *110*, 272.

(14) Hirai, H.; Wada, K.; Kurima, K.; Komiyama, M. Carbon Monoxide Adsorbent Composed of Copper(I) Chloride and Polystyrene Resin Having Amino Groups. *Bull. Chem. Soc. Jpn.* **1986**, *59*, 2553.

(15) Yin, Y.; Tan, P.; Liu, X.-Q.; Zhu, J.; Sun, L.-B. Constructing a Confined Space in Silica Nanopores: an ideal Platform for the Formation and Dispersion of Cuprous Sites. *J. Mater. Chem. A* **2014**, *2*, 3399.

(16) Wang, Y.; Yang, R. T.; Heinzel, J. M. Desulfurization of Jet Fuel by π-Complexation Adsorption with Metal Halides Supported on MCM-41 and SBA-15 Mesoporous Materials. *Chem. Eng. Sci.* **2008**, *63*, 356.